

Modeling a Submicrometer Electrostatic Motor

J. H. Wright,^{*,†} D. P. Sheehan,[‡] and A. R. Putnam[‡]

[†] Department of Mathematics and Computer Science, University of San Diego, San Diego, California 92110, USA

[‡] Department of Physics, University of San Diego, San Diego, California 92110, USA

Numerical models are developed for a recently proposed submicrometer device that uses the electric field energy of a biased parallel-plate semiconducting capacitor to propel a piston through the open capacitor gap. Through variation of design parameters or applied external bias, actuator forces on the order of hundreds of piconewtons are developed for device size scales ranging from 10^{-7} m to 10^{-4} m per side. A rotary configuration of the device is also presented.

Keywords: Nanotechnology, Linear, Rotary, Actuator, Electrostatic, MEMS, NEMS.

1. INTRODUCTION

A key to the further development of mature MEMS and NEMS technology will be the availability of robust actuators and motors. This paper introduces the numerical modeling of a class of devices that has recently been proposed¹ to generate mechanical motion by harnessing a dynamic instability associated with the electric field of the open gap of a biased parallel-plate semiconducting capacitor. The paper is organized as follows: first, the device is described and the physical principles leading to the dynamic instability are presented. Models for various aspects of the engineering challenges and numerical estimates of actuator forces are developed. Finally, a rotary device that operates on the same principles is described.

Consider a microscale channel formed by two parallel slabs of doped silicon spaced a distance l_x apart and biased with a voltage V_b . Because of the arrested diffusion of charge carriers across the open gap, V_b is expressed mainly across the vacuum gap. This configuration constitutes a parallel-plate capacitor in which the plates are semiconducting, rather than conducting. For fixed voltage, the electric field strength is inversely proportional to the channel width. As shown in Figure 1, a slab of semiconducting dielectric material, called a *piston* or a *nanopiston*, slides in the gap. The piston is initially drawn into the gap by the strong electric field gradient there, while maintaining physical and electrical contact with both walls on either side of the gap.

In contrast to the principle of operation of interdigitated electrostatic actuators,² where the electrostatic attraction of charged capacitor plates is harnessed to produce an actuator force, the operation of this device is based on the $\mathbf{P} \cdot \nabla \mathbf{E}$ force that pulls a dielectric slab into a fringing electric field. As the piston slides through the gap it locally

shorts out the gap walls, providing a semiconducting circuit by which charge can flow across the gap. Numerical modeling with commercial simulators¹ indicates that the semiconducting material of the walls and the piston supports finite, but short-lived, surface charge gradients. As long as the piston makes physical contact between points on opposing gap walls, charge flows from one side to the other, locally reducing the charge density with exponential time constant τ_d . Furthermore, again because of the semiconducting properties of the materials, once the piston passes and is no longer in contact, the gap walls recharge from the external bias with time constant τ_r . The result is that the field ahead of the moving piston is unperturbed and stronger than the diminished field behind the piston. The piston hence experiences a constant net $\mathbf{P} \cdot \nabla \mathbf{E}$ force in the forward direction of its motion. In effect, the piston surfs a minimum in electrostatic energy of its own making through the channel.

This effect only applies when the material of the walls and the piston is semiconducting. For perfect conductors, $\tau_d \rightarrow 0$, and current flow is instantaneous, shorting out the entire gap walls so that no unbalanced field, indeed no field at all, would be supported. With insulators, on the other hand, $\tau_d \rightarrow \infty$, and no discharge current could flow that would establish a difference in field strength, and hence a net force, between the leading and trailing faces of the piston.

The force acting on the *nanopiston* is the electrostatic analog of the attraction of a ferromagnetic slab into a magnetic field, found by integrating the value of $\mathbf{M} \cdot \nabla \mathbf{B}$ over the volume of the slab. The device considered here can also be considered the electrostatic analog of the well-known magnetic rail gun, but operates at a much smaller scale. As a result, there are a number of potential applications that have yet to be considered.

A further goal of this work is to model the physics of biasing the gap (and hence powering the motion of the

* Author to whom correspondence should be addressed.

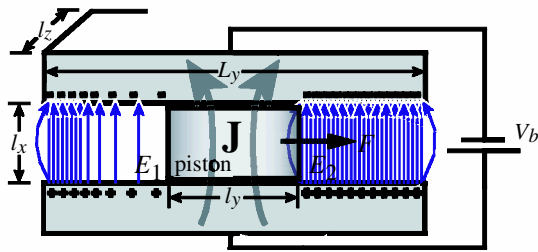


Fig. 1. Overview of the dynamic instability of the *nanopiston*. J represents the current density flowing through the piston connecting the lower and upper gap faces; E_1 and E_2 are the trailing and leading electric field strengths, respectively; and F is the net electrostatic force exerted on the piston in the direction of its travel. V_b is the applied bias voltage.

piston through the gap) by means of the potential difference associated with the depletion region of a p-n junction, as depicted in Figure 2. This figure shows a silicon device in the shape of a horseshoe and doped with n-type impurities on the left side and p-type impurities on the right side. In the upper region, the n and p regions are in physical contact, while in the lower region they are separated by a vacuum gap. The thermal generation of carriers resulting in a depletion region across the continuous p-n junction in the upper region gives rise to a bias voltage across the discontinuous vacuum gap in the lower region.¹ As with the case of the externally biased device, these thermally generated charge carriers accumulate near the gap walls and are available for discharge by the passing piston.

2. NUMERICAL MODELS

Two distinct numerical models for the operation of the nanopiston are considered here. The first is a two-dimensional simulation performed with standard commercial semiconductor simulation software that yields the total electrostatic energy associated with the piston statically occupying various positions within the gap.

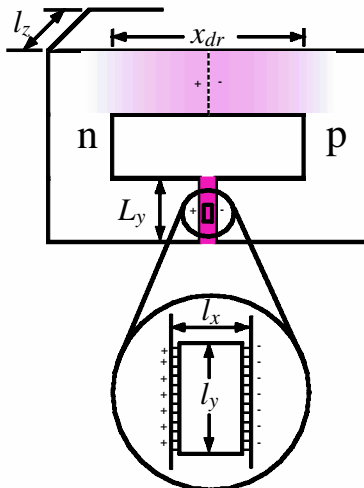


Fig. 2. Schematic of the nanopiston device with gap voltage provided by the built-in potential difference of the p-n junction.

The results of this model suggest that energy in the depletion region of the p-n junction diode should be available for capture by the piston as it moves into and through the gap. Furthermore, the model gives insight into the role of the geometry of the depletion region as a mechanism for focusing electrostatic energy into the vacuum gap.

Motivated by the two-dimensional model for static pistons, the one-dimensional model seeks to quantify the forces and accelerations experienced by a piston moving at constant velocity through a fully charged gap, and to provide a means of estimating when the electrostatic force can overcome friction and stiction.

2.1. 2-D Model

Figure 3 displays the equilibrium electrostatic energies of the device and piston pictured in Figure 2 for a sequence of piston positions within the gap. These simulations were performed with Silvaco International’s semiconductor Device Simulation Software [Atlas (S-Pisces, Giga)]. The dimensions of the configuration were channel length $L_y = 3000 \text{ \AA}$, and the piston dimensions were $l_x = 300 \text{ \AA}$ by $l_y = 600 \text{ \AA}$. The junctions were modeled as abrupt with doping levels $N_A = N_D = 10^{15} \text{ cm}^{-3}$, and the physical parameters for charge carriers were generic, resulting in a bias voltage of $V_{bi} = 0.6 \text{ V}$. A nanopiston with these physical dimensions will henceforth be referred to as the *standard device*. Output from the Silvaco simulations was the two-dimensional, steady-state, simultaneous solutions to the Poisson, continuity, and force equations, obtained with the Shockley-Read-Hall recombination model. Vacuum gap energies were calculated as $\epsilon_o E^2/2$, and silicon bulk energies were found using $\mathbf{D} \cdot \mathbf{E}/2$.

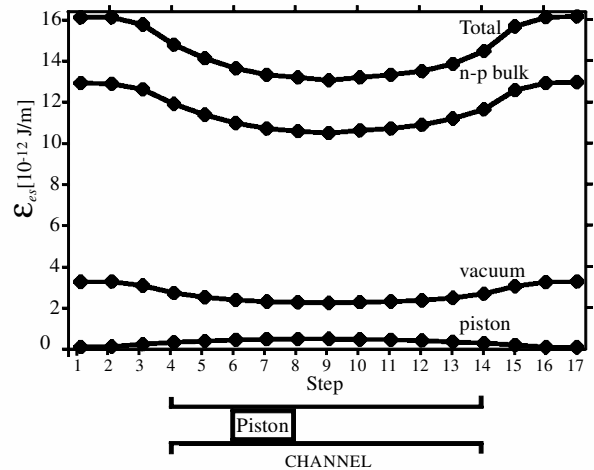


Fig. 3. Energy levels associated with various positions of the piston within the gap. Full electrical contact between the piston and the gap walls is assumed for each step, and the piston is assumed to be stationary. The total energy shown is the sum of the electrostatic energy of the field within the vacuum gap as well as the polarization and field energy of the silicon bulk and the piston.

Figure 3 indicates that the total, vacuum gap, and p-n bulk energies decrease significantly and symmetrically as the piston is placed at various positions in the channel, ranging from fully outside the gap (Steps 1 and 17) and reaching to mid-channel (Step 9). The greatest absolute change occurs in the bulk. The electrostatic energy invested in the piston itself actually increases as the piston occupies positions near the center of the gap, but the increase is small compared with the decrease seen in the bulk and vacuum energies and suggests that the piston plays a role in changing the electrostatic geometry of the device without itself storing a significant amount of energy. A numerical differentiation of the data of Figure 3 suggests that, if surface forces can be overcome, electric field and bulk polarization energy should be converted into the kinetic energy of the piston as the piston moves into the high-intensity region in the interior of the gap.

The range of sizes over which the device could operate is closely related to the width of the depletion region at various doping levels. To find the total electrostatic energy available for harvest, we estimate the electrostatic energy associated with the gap region of the device in two limiting cases: with the channel fully open and fully closed (i.e., no channel at all). In the open case, the energy of the gap is found purely from the field energy of the capacitor consisting of the charged open-gap walls; in the closed-gap case, the energy is the field and polarization energy across the entire depletion region. (It was found in calculations performed using the Silvaco-Atlas software and reported elsewhere¹ that the E -field in the gap region saturates at approximately 2×10^5 V/cm. Above this intensity, a gradient of charge density, and hence energy, extends back from the gap walls into the silicon bulk, reducing the effect of the piston on the total energy of the system as it occupies various positions within the gap. The configurations considered here were chosen to avoid this saturation limit.)

The intrinsic bias V_{bi} and width of the depletion region x_{dr} may be estimated by^{3, 4}

$$V_{bi} = \frac{kT}{q} \ln\left(\frac{N_A N_D}{n_i^2}\right) \quad (1)$$

and

$$x_{dr} = \left[\frac{2\kappa\epsilon_o V_{bi} (N_A + N_D)}{q N_A N_D} \right]^{1/2} \quad (2)$$

where kT is the thermal energy, q is an electronic charge, n_i is the intrinsic carrier concentration of silicon ($n_i \approx 1.2 \times 10^{10}$ cm⁻³ at 300 K), ϵ_o is the permittivity of free space, and $\kappa = 11.8$ is the dielectric constant for silicon.

We take $N_A = N_D = N$, and combine Eqs. (1) and (2) and the energy contained in a parallel-plate capacitor with plates spaced a distance l_x apart to obtain an estimate of

the difference in energy between open-gap and closed-gap configurations as a function of dopant concentration N :

$$\Delta \mathcal{E}_{es} \approx \frac{16\kappa\epsilon_o^2}{qN} \left\{ \frac{kT}{q} \ln\left[\frac{N}{n_i}\right] \right\}^3 \left\{ \frac{1}{l_x} - \frac{q}{3} \sqrt{\frac{\kappa N}{kT\epsilon_o \ln[N/n_i]}} \right\} \quad (3)$$

It is evident from (3) that the energy of the device varies strongly with temperature, scaling as $(T)^3$. This is not surprising since the primary determinants of the energy are V_{bi} and x_{dr} , both of which originate from thermal processes. Of more interest in the current discussion, however, is the complicated scaling of the available energy with the doping N , for this gives an indication of the overall scales that may be considered when actually engineering a device.

Figure 4 displays the difference predicted by (3) of the energy between open-gap and closed-gap configurations for a range of doping levels (affecting primarily x_{dr}) and gap widths l_x . The plot shows a general increase in the available energy as the doping is decreased, with the maximum energy available at intrinsic levels. In the region labeled *endothermic gap closing* the energy of the open-gap configuration is actually lower than the closed-gap configuration, so that energy would have to be supplied to drive the piston into the gap. This is consistent with the minus sign on the right-hand side of (3).

This model depends strongly on the width of the depletion region at small dopant concentrations (as predicted by (2)). As the dopant concentration varies below about 10^{15} cm⁻³, Figure 5 shows that the depletion region grows rapidly to orders of magnitude larger than the device. Before the onset of this nonphysical prediction, however, we observe a regime in which the depletion region is on the same scale as the overall device dimensions. Lowering dopant concentrations to this level reduces gap-region

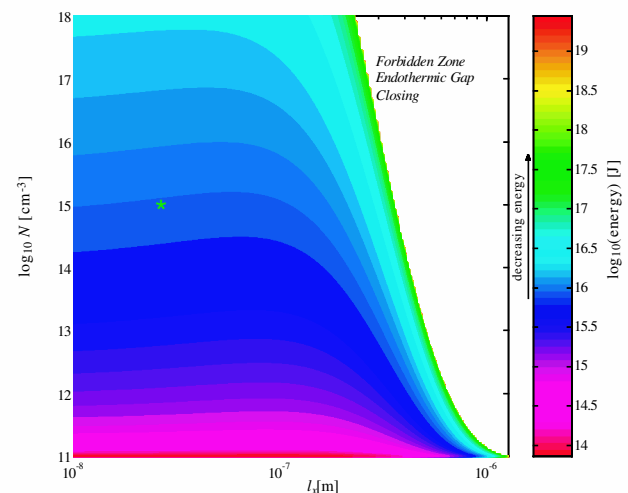


Fig. 4. Energy difference calculated from Eq. (3) between open-gap and closed-gap configurations of the devices geometrically scaled as the *standard device*, as the gap width l_x is scaled logarithmically from 30 nm to 1000 nm and doping is varied from $N = 10^{11}$ cm⁻³ to $N = 10^{18}$ cm⁻³.

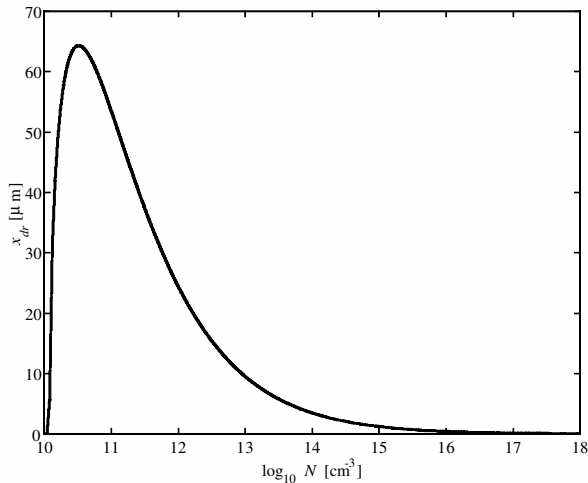


Fig. 5. Dependence of depletion region width x_{dr} on dopant concentration. The size predicted for the depletion region depends on the dopant concentration alone.

energy in the closed-gap case, while still allowing a high energy density within the gap region in the open-gap case. As the size of the gap (and the piston within it) grows to reach the scale of the depletion region, the effect of the piston on the vacuum field decreases, so that the majority of the difference in energy between the in-gap and out-of-gap configurations may be accounted for by changes in the bulk energy density of the piston itself as it polarizes, with minimal contributions from the vacuum and bulk energies. This result suggests that the device works only for gap widths that are small compared with the width of the depletion region.

2.2. 1-D Model

Building on the results of the static 2-D model, we wish to take advantage of reasonable simplifying assumptions regarding electrodynamic and thermodynamic phenomena within the bulk and the gap to capture the essential dynamics of the device. This model seeks to develop a means of estimating the dynamic balance between electromotive forces and frictional and loading counter-forces.

We assume the gap to be of infinite length, the electric field intensity E in the gap to be scalar valued, that E arises from the accumulation of charge on the surfaces of the open gap, and that this charge is supplied either by the depletion region of the p-n junction or by an external bias. Beyond the thermal generation of the depletion region and its concomitant field across the gap, we do not consider thermal effects.

Application of the method of virtual work allows the net force on the piston to be estimated by examining the change in the energy as the piston is driven *at constant velocity* through the gap. The assumption of constant velocity is that of quasi-equilibrium: it allows the easy calculation of leading and trailing electric field

strengths based on exponential decay of surface charge. This approach meets the aims of the model while avoiding the more computationally involved reference to the $\mathbf{P} \cdot \nabla \mathbf{E}$ body forces that explicitly give rise to the force on the piston. The energy difference arises as a result of the imbalance in the electric fields E_1 and E_2 on either end of the piston. With these assumptions, the electrostatic acceleration felt by the piston is given by³

$$a_{es} = \frac{\epsilon_o \chi_e (E_2^2 - E_1^2)}{2\rho_{si} l_y} \quad (4)$$

where ϵ_o is the permittivity of free space, and ρ_{si} and χ_e are the mass density and electric susceptibility, respectively, of silicon.

It is well known that, at micrometer and submicrometer size scales, atomic, ionic, and electrostatic forces (e.g., van der Waals interactions, induced surface charge, molecular and hydrogen bonding, surface tension) can play dominant roles in system dynamics.⁵ To model the sliding friction between the piston faces and gap walls, we suppose all surfaces in contact to be tiled with a thin, low-friction surface such as graphite. We further require that the tiling be only partial, so that the contact fraction, f_c , between the piston and the channel walls is small ($0 < f_c \sim 1$). On the other hand, f_c must be large enough to provide adequate contact between the piston surfaces and the channel walls both to hold and guide the piston, and to provide sufficiently good electrical contact between the piston and the channel walls to allow the use of standard Ohmic current rather than quantum mechanical tunneling current to describe the system's electrical behavior (atomically flat layers required by the device are on the horizon).

The smallest nonzero coefficients of static and kinetic friction yet measured experimentally have been found in nested multiwalled carbon nanotubes (MWNTs).^{6–9} Upper-limit values of coefficients of static (s) and kinetic (k) friction have been experimentally measured to be $\mathcal{F}_s < 2.3 \times 10^{-14}$ N/atom = 6.6×10^5 N/m², and $\mathcal{F}_k < 1.5 \times 10^{-14}$ N/atom = 4.3×10^5 N/m². Furthermore, experimental observations suggest that MWNTs may be utilized as totally wear-free bearings.⁶

The frictional force can be expressed as $2\mathcal{F}_s f_c l_y l_z$, where the product $2l_y l_z$ is the total area of the faces of the piston that are in contact with the gap walls. The total force on the piston is then estimated by

$$F = \frac{1}{2} \epsilon_o l_x l_z \chi_e [E_2^2 - E_1^2] - 2\mathcal{F}_s f_c l_y l_z \quad (5)$$

where the variables are given in Figure 1, and l_z is the depth of the device in the z dimension.

To evaluate the utility of the device as a linear actuator or motor, in Figure 6 we present estimates of the net force predicted by Eq. (5) exerted on pistons over a range of device scalings and operating velocities. For this figure, we assume that the piston is sliding through gaps with

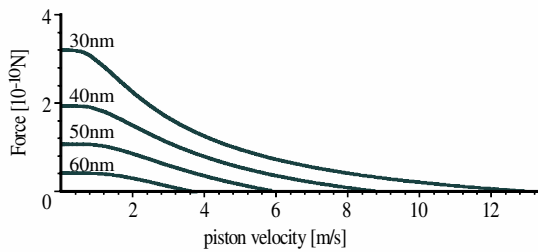


Fig. 6. Total force in excess of friction developed by piston scaled as the standard device for gap widths indicated on each curve. The piston width l_x is taken equal to the gap width, piston length $l_y = 2l_x$, and constant piston depth $l_z = 1 \mu\text{m}$.

widths ranging from 30 nm to 60 nm, at constant velocity v indicated on the x axis; the charge located at opposite points on gap walls flows through the piston while it is in contact, allowing the field strength E_1 to decay with an exponential time constant τ_d consistent with dopant levels for the time $t = L_y/v$ that contact is maintained between opposed points on the gap walls; conservative values for static friction ($\mathcal{F}_s = 6.6 \times 10^5 \text{ N/m}^2$) and surface coverage fraction ($f_c = 0.2\%$); and the fact that the field strength in the direction of piston motion is that of a saturated capacitor field, $E_2 = V_b/l_x$. We note also that gap widths smaller than 30 nm, while conceivable to build, in the case of intrinsic diode bias would result in electric field strengths in excess of the $2 \times 10^5 \text{ V/cm}$ saturation limit, and hence are not considered in this model. The forces, on the order of hundreds of piconewtons for the device ranges considered here at overall device scalings of approximately $1 \mu\text{m}$, can be compared with molecular motors in biotic systems^{10, 11} that exhibit forces on the order of tens of piconewtons at similar scalings.

The schematic of a radially symmetric version of the linear device is shown in Figure 7. The device consists of a slab of silicon of height l_z with a circular vacuum channel of depth l_z , radius r_0 , and width l_x etched in the top. The device is lightly doped with acceptor impurities in the region $r < r_0$ and donor impurities in the region $r > r_0$. The doping concentrations are the same as for the linear device, and the size of the depletion region (Eq. (2)) of the resulting p-n diode junction $x_{dr} \approx r_0$. For the doping shown in the diagram, the n-region is toroidal in shape, while the p-region is cylindrical. The physical continuity of the n- and p-regions at the radius r_0 and below the gap depth l_z results in a radially symmetric depletion region with bias voltage expressed across the gap at depths less than l_z .

In the bottom part of the device, where the p- and n-regions are in physical contact, a depletion region in the physical shape of an annulus forms, whereas in the upper part of the device, the p- and n-regions are separated by a vacuum gap of width l_x . The electrostatic potential

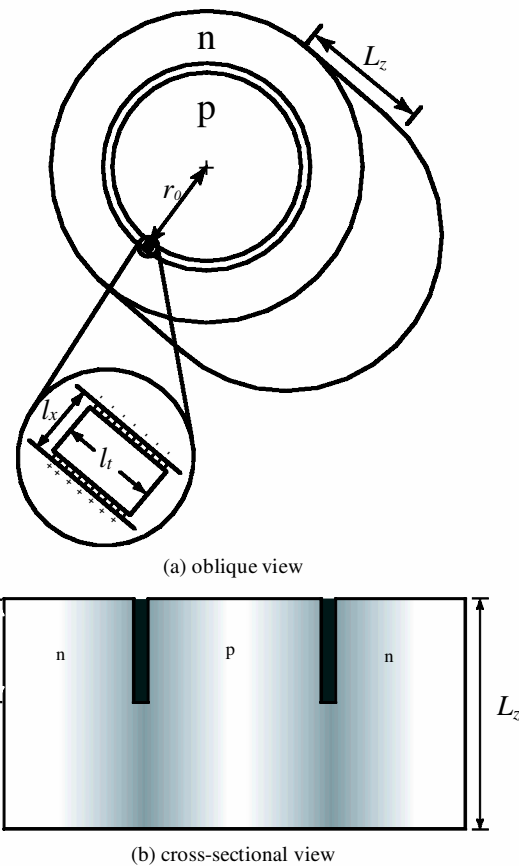


Fig. 7. Schematic diagram of rotary electrostatic motor. (a) Oblique view. (b) Cross-sectional view.

difference naturally arising through the depletion region is expressed as a high-intensity electric field in the gap region. To avoid complications arising from interactions of the radially symmetric geometry both in the presence of non-uniform fringing fields in the channel due to curved channel walls, and in the action and fit of the rectangular piston traveling within the curved channel walls, we assume that the local action of the piston in the gap is adequately replicated by the linear results. This assumption requires that the rotor radius be greater than the channel width by roughly an order of magnitude or more.

3. SUMMARY

We have presented various models for a new class of mesoscopic devices that could provide linear and rotary locomotion at small scales. These could be an important new resource for designers of small-scale systems. Besides these practical results, the concept of this design also raises fundamental questions in the relation and balance between electrical, mechanical, and thermal forms of energy at this scale and will be the basis of future research.

Acknowledgments: The authors thank the reviewers for their insightful and helpful comments.

References and Notes

1. D. P. Sheehan, A. N. Putnam, and J. H. Wright, *Found. Phys.* 35 (2002).
2. N. C. MacDonald, in *Nanotechnology*, A.I.P. Press, New York (1999), chap. 3.
3. D. J. Griffiths, in *Introduction to Electrodynamics*, Prentice Hall, Upper Saddle River, NJ (1999), pp. 194–196.
4. J. S. Yuan and J. J. Liou, *Semiconductor Device Physics and Simulation*, Plenum, New York (1998).
5. D. Bishop, P. Gammel, and C. R. Giles, *Physics Today* 54 (2001).
6. J. Cumings and A. Zettl, *Science* 289, 602 (2000).
7. Y. Min-Feng, B. I. Yakobson, and R. S. Ruoff, *J. Phys. Chem.* 104, 8764 (2000).
8. M. S. Dresselhaus, G. Dresselhaus, and P. Avouris, editors, *Carbon Nanotubes—Synthesis, Structure, Properties and Applications*, Springer-Verlag, Berlin (2001).
9. P. J. F. Harris, *Carbon Nanotubes and Related Structures*, Cambridge University Press, Cambridge, UK (1999).
10. Douglas E. Smith, Sander J. Tans, Steven B. Smith, Shelley Grimes, Dwight L. Anderson, and Carlos Bustamante, *Nature* 413, 748 (2001).
11. Alan A. Simpson, Yizhi Tao, Petr G. Leiman, Mohammed O. Badasso, Yongning He, Paul J. Jardine, Norman H. Olson, Marc C. Morals, Shelley Grimes, Dwight L. Anderson, Timothy S. Baker, and Michael G. Rossman, *Nature* 408, 745 (2000).

Received: 12 November 2002. Revised/Accepted: 18 March 2003.